

Neutral Higgs boson pair production in photon-photon annihilation in the Two Higgs Doublet Model

Abdesslam Arhrib^{1,2}, Rachid Benbrik^{2,3,4}, Chuan-Hung Chen^{3,4} and Rui Santos⁵

¹ *Département de Mathématique, Faculté des Sciences and Techniques,
Université Abdelmalek Essaâdi, B. 416, Tangier, Morocco.*

² *LPHEA, Faculté des Sciences-Semlalia, B.P. 2390 Marrakesh, Morocco.*

³ *Department of Physics, National Cheng Kung University, Taiwan 701, Taiwan.*

⁴ *National Center for Theoretical Physics, Taiwan 701, Taiwan. and*

⁵ *NExT Institute and School of Physics and Astronomy,
University of Southampton Highfield, Southampton SO17 1BJ, UK.*

(Dated: February 6, 2020)

Abstract

We study double Higgs production in photon-photon collisions as a probe of the new dynamics of Higgs interactions in the framework of two Higgs Doublet Models. We analyze neutral Higgs bosons production and decay in the fusion processes, $\gamma\gamma \rightarrow S_i S_j$, $S_i = h^0, H^0, A^0$, and show that both $h^0 h^0$ and $A^0 A^0$ production can be enhanced by threshold effects in the region $E_{\gamma\gamma} \approx 2m_{H^\pm}$. Resonant effects due to the heavy Higgs, H^0 , can also play an important role in the cross section enhancement when it is allowed to decay to two light CP-even h^0 or to two light CP-odd A^0 scalars. We find that the total cross sections are very sensitive to the Two Higgs Doublet Model parameters, and that they are typically one to three orders of magnitude above the Standard Model cross section for Higgs pair production via photon fusion. We also present and discuss the angular distributions for CP-even and CP-odd final states. We further show that photon-photon collisions provide an important means to determine triple Higgs interactions and could distinguish between the Standard Model and the Two Higgs Doublet Model predictions.

PACS numbers: 12.60.Fr, 14.80.Cp

I. INTRODUCTION

The search for Higgs bosons is the prime task of CERN's Large Hadron Collider (LHC), with operation scheduled now for 2009. With the LHC guidance, the International e^+e^- Linear Collider (ILC), which is currently being designed, will further improve our knowledge of the Higgs sector if that is how Nature decided to create mass. It was demonstrated in Ref. [1] that physics at the LHC and at the ILC will be complementary to each other in many respects. In many cases, the ILC can significantly improve the LHC measurements. If a Higgs boson is discovered, it will be crucial to determine its couplings with high accuracy, to understand the so-called mechanism of electroweak symmetry breaking [2]. The high resolution profile determination of a light Higgs boson (mass, couplings, self couplings, etc.) can be carried out at the ILC, where clear signals of Higgs events are expected with backgrounds that can be reduced to a manageable level. This is exactly the case of processes such as $e^+e^- \rightarrow \gamma\gamma \rightarrow S_i S_j$ where $S_i = h^0, H^0, A^0$. This fusion process can produce a Standard Model (SM) Higgs boson or one predicted by the various extensions of the SM, such as the Minimal Supersymmetric Standard Model (MSSM) or Two Higgs Doublet Models (2HDM).

According to its Reference Design Report [3], the ILC will run at an energy of $\sqrt{s} = 500$ GeV with a total luminosity of $\mathcal{L} = 500 fb^{-1}$ within the first four years of operation and $\mathcal{L} = 1000 fb^{-1}$ during the first phase of operation with $\sqrt{s} = 500$ GeV. An e^+e^- collider is uniquely capable of operation at a series of energies near the threshold of a new physics process. This is an extremely powerful tool for precision measurements of particle masses and unambiguous particle spin determination. Various ILC physics studies, indicate that a $\sqrt{s} = 500$ GeV collider can have a great impact on understanding new physics at the TeV scale. An energy upgrade up to $\sqrt{s} \sim 1$ TeV would open the door to even greater discoveries. Another very unique feature of the ILC is that it can be transformed into a $\gamma\gamma$ collider with the photon beams generated by using the Compton backscattering of the initial electron and laser beams [4]. In this case, the energy and luminosity of the photon beams would be of the same order of magnitude of the original electron beams. As the set of final states at a photon collider is much richer than that in the e^+e^- mode, it would open a wider window to probe new physics beyond the SM.

Since photons couple directly to all fundamental fields carrying electromagnetic charge, $\gamma\gamma$ collisions provide a comprehensive means of exploring virtual aspect of the SM and its

extensions [5]. The production mechanism in hadron and e^+e^- machines are often more complex and model-dependent. Thus, a $\gamma\gamma$ collider is much more sensitive to new physics even at higher mass scales [6].

The primary mechanism of neutral Higgs boson production in $\gamma\gamma$ collisions is $\gamma\gamma \rightarrow (h^0, H^0, A^0)$ [7, 8, 9, 10], but in order to explore the triple and quartic Higgs couplings at future high energy colliders, it is necessary to study the Higgs boson pair production process. The triple Higgs couplings of the 2HDM have been extensively studied at e^+e^- linear colliders [11] and shown to provide an opportunity to measure those couplings. At photon-photon colliders, the cross section for neutral Higgs boson pair production has been calculated in [12, 13] in the SM and found to be rather small. In the 2HDM, the process $\gamma\gamma \rightarrow h^0 h^0$ has been computed in the decoupling limit in [14, 15]. They found that the cross section can be substantially enhanced in the 2HDM and that the number of events expected at the Photon Collider will allow a determination or exclusion of some of the parameter space in the 2HDM potential.

In the MSSM, various studies for Higgs pair production at a photon collider have been performed. The process $\gamma\gamma \rightarrow h^0 h^0$ was studied in [16] while reactions $\gamma\gamma \rightarrow h^0 H^0, h^0 A^0, H^0 H^0, H^0 A^0$ were determined in [17]. Process $\gamma\gamma \rightarrow A^0 A^0$ was calculated for the MSSM [18, 19] and shown to have a cross section of the order of $0.1 - 0.2 \text{ fb}$ for a vast range of the photon-photon center-of-mass energy.

In this paper, we present a complete calculation of pair production of all neutral Higgs bosons at the one loop level in the 2HDM. We study the self Higgs couplings effects on the $\gamma\gamma \rightarrow h^0 h^0$, $\gamma\gamma \rightarrow A^0 A^0$ and $\gamma\gamma \rightarrow h^0 A^0$ cross sections and briefly comment on the $\gamma\gamma \rightarrow h^0 H^0$, $\gamma\gamma \rightarrow H^0 A^0$ and $\gamma\gamma \rightarrow H^0 H^0$ production modes. This exhausts all possible neutral scalar production processes in the 2HDM. A measurement of these processes can shed some light on the 2HDM triple Higgs couplings. The scalars will be detected via similar final states because both the h^0 and the A^0 , when not too heavy, decay predominantly into fermions. In this regard, the knowledge of their exact total cross section and angular distributions may be helpful in order to distinguish between CP-even and CP-odd scalars. Moreover, it is well-known that in the 2HDM, both the CP-even h^0 and the CP-odd pseudo-scalar A^0 can be rather light [20]. In fact, the bounds on the h^0 and A^0 masses originate from the $e^+e^- \rightarrow h^0 Z$ and $e^+e^- \rightarrow h^0 A^0$ production processes with the Higgs decaying to some combination of jets (mainly b jets) and τ leptons. The production process $e^+e^- \rightarrow h^0 Z$

is proportional to $\sin^2(\alpha - \beta)$ and this is the reason why LEP does not limit the mass of a light Higgs h^0 for $\sin(\alpha - \beta) = 0.1$. For $\sin(\alpha - \beta) = 0.3$ the bound is of the order of 80 *GeV*. The pseudo-scalar mass is only limited by the results on $e^+e^- \rightarrow h^0 A^0$. However, if the sum of the masses is above the LEP energy limit, again no bound applies.

A very interesting feature of $\gamma\gamma \rightarrow A^0 A^0$ is that a light A^0 can easily emerge in the Next-to Minimal Supersymmetric Standard Model (NMSSM) and therefore comparison between models will certainly prove useful. In addition, we also take into account in our calculation the perturbativity as well as vacuum stability constraints on the various parameters in the Higgs potential. We will show that after imposing those constraints, cross sections are still large enough, a few pico-barn (*pb*) in some cases, to allow for a determination of the 2HDM triple Higgs couplings. We will also study some of these processes in the decoupling limit and in the fermiophobic limit of the so-called type-I 2HDM.

The paper is organized as follows. In the next section, we review the 2HDM potential and give the analytical expression of triple and quartic Higgs couplings. In Section III, we evaluate the double Higgs production cross section, $\gamma\gamma \rightarrow S_i S_j$ with $S_{i,j} = H^0, h^0, A^0$, in the general 2HDM paying special attention to $\gamma\gamma \rightarrow h^0 h^0$ and $\gamma\gamma \rightarrow A^0 A^0$. We then proceed to Section IV where we present our numerical results for the general 2HDM and for two limiting cases: the decoupling limit and the fermiophobic limit. In Section V we discuss the final states in the different 2HDM scenarios. Our findings are summarized in Section VI.

II. REVIEW OF THE TWO HIGGS DOUBLET MODEL

A. The Two Higgs doublet model

Two Higgs doublet models are some of the most well studied extensions of the Standard Model. Various motivations for adding a second Higgs doublet to the Standard Model have been advocated in the literature [21, 22]. There are several types of 2HDM. While the coupling to gauge bosons is universal, there are many ways to couple the Higgs doublets to matter fields. Assuming natural flavor conservation [23] there are four ways to couple the Higgs to fermions [24]. The most popular models are the type-I and the type-II models, denoted by 2HDM-I and 2HDM-II, respectively. In 2HDM-I, the quarks and leptons couple only to one of the two Higgs doublet which is exactly what happens in the SM. In 2HDM-II,

one of the 2HDM fields couples only to down-type fermions (down-type quarks and charged leptons) and the other one only couples to up-type fermions in order to avoid the problem of flavor-changing neutral currents (FCNC's) at tree-level. A class of models sometimes called type-III and denoted as 2HDM-III have FCNC induced at tree-level [25] which can lead to fine-tuning issues. The discussion of the different models is not crucial as the production processes discussed here have a very mild dependence on the diagrams with fermion loops. It can however become relevant when discussing the different final states. When the Higgs decays predominantly to fermions, the relative size of the $h^0 \rightarrow b\bar{b}$, $h^0 \rightarrow c\bar{c}$ and $h^0 \rightarrow \tau^+\tau^-$ branching ratios do depend on the model chosen regarding the Yukawa sector. Finally, we note that a 2HDM-I can lead to a fermiophobic Higgs boson h^0 [26] with suppressed couplings to the fermions (exactly zero at tree-level). In this case, the dominant decay mode for the lightest Higgs boson is $h^0 \rightarrow \gamma\gamma$ or $h^0 \rightarrow W^+W^-$, depending on its mass. No other version of the 2HDM possesses such a feature.

The most general scalar potential, renormalizable, CP-conserving, invariant under $SU(2)_L \otimes U(1)_Y$ can be written as [21]:

$$\begin{aligned} V(\Phi_1, \Phi_2) = & m_1^2 \Phi_1^\dagger \Phi_1 + m_2^2 \Phi_2^\dagger \Phi_2 - (m_{12}^2 \Phi_1^\dagger \Phi_2 + \text{h.c.}) + \frac{1}{2} \lambda_1 (\Phi_1^\dagger \Phi_1)^2 + \frac{1}{2} \lambda_2 (\Phi_2^\dagger \Phi_2)^2 \\ & + \lambda_3 (\Phi_1^\dagger \Phi_1) (\Phi_2^\dagger \Phi_2) + \lambda_4 (\Phi_1^\dagger \Phi_2) (\Phi_1^\dagger \Phi_2) + \frac{1}{2} \lambda_5 [(\Phi_1^\dagger \Phi_2)^2 + \text{h.c.}] , \end{aligned} \quad (1)$$

where Φ_1 and Φ_2 have weak hypercharge $Y = 1$ and vacuum expectation values (VEV's) v_1 and v_2 , respectively, and λ_i and m_{12} are real-valued parameters. Note that this potential violates the discrete symmetry $\Phi_i \rightarrow -\Phi_i$ softly by the dimension-two term $m_{12}^2 (\Phi_1^\dagger \Phi_2)$, and has the same general structure as the scalar potential in the MSSM.

After electroweak symmetry breaking, the W^\pm and Z gauge bosons acquire their masses. Explicitly, three of the eight degrees of freedom in the two Higgs doublets correspond to the three Goldstone bosons (G^\pm, G^0) and the remaining five become physical Higgs bosons: h^0 , H^0 (CP-even), A^0 (CP-odd), and H^\pm with masses m_{h^0} , m_{H^0} , m_{A^0} , and m_{H^\pm} , respectively.

The potential in Eq. (1) has ten independent parameters (including v_1 and v_2). The parameters m_1 and m_2 are fixed by the minimization conditions. The combination $v^2 = v_1^2 + v_2^2$ is fixed as usual by the electroweak breaking scale through $v^2 = (2\sqrt{2}G_F)^{-1}$. We are thus left with seven independent parameters; namely $(\lambda_i)_{i=1,\dots,5}$, m_{12} , and $\tan \beta \equiv v_2/v_1$. Equivalently, we can take instead

$$m_{h^0} \quad , \quad m_{H^0} \quad , \quad m_{A^0} \quad , \quad m_{H^\pm} \quad , \quad \tan \beta \quad , \quad \alpha \quad \text{and} \quad m_{12} \quad , \quad (2)$$

as the seven independent parameters. The angle β diagonalizes both the CP-odd and charged scalar mass matrices and α diagonalizes the CP-even mass matrix. One can easily relate the physical scalar masses and mixing angles from Eq. (1) to the potential parameters, λ_i , m_{12} and v_i , and invert them to obtain λ_i in terms of the physical scalar masses, $\tan\beta$, α , and m_{12} [27, 28].

B. Theoretical and experimental constraints

There are several important constraints on the 2HDM parameters imposed by experimental data. In our analysis we take into account all available experimental constraints when the independent parameters are varied.

First, the LEP direct search result in the lower bounds $m_{h^0} > 114 \text{ GeV}$ for a SM-like Higgs and $m_{A^0, H^0, H^\pm} > 80\text{-}90 \text{ GeV}$ for supersymmetric models in the case of the neutral scalars and for more general models in the case of the charged Higgs (see [29] for details). As stated in the introduction, the bound on the lightest CP-even Higgs heavily depends on the value of $\sin(\alpha - \beta)$. In a general 2HDM all bounds on the Higgs masses, with the exception of the charged Higgs, can be avoided with a suitable choice of the angles and m_{12} .

Second, the extra contributions to the $\Delta\rho$ parameter from the Higgs scalars [30] should not exceed the current limit from precision measurements [29]: $|\Delta\rho| \lesssim 10^{-3}$. Such an extra contribution to $\delta\rho$ vanishes in the limit $m_{H^\pm} = m_{A^0}$. To ensure that $\Delta\rho$ is within the allowed range, we demand either a small splitting between m_{H^\pm} and m_{A^0} or a combination of parameters that produces the same effect.

Third, the constraint from $B \rightarrow X_s \gamma$ branching ratio [31, 32] gives a lower bound on the charged Higgs mass, $m_{H^\pm} \gtrsim 295 \text{ GeV}$, in 2HDM-II. These bounds do not apply to model type-I and therefore are not taken into account in the fermiophobic scenario. Recent data from $B \rightarrow \ell \nu$ can also give a constraint on charged Higgs mass especially for large values of $\tan\beta$ in 2HDM-II [33, 34].

Fourth, values of $\tan\beta$ smaller than ≈ 1 are disallowed both by the constraints coming from $Z \rightarrow b\bar{b}$ and from $B_q \bar{B}_q$ mixing [31].

Finally, we should take into account the theoretical constraints. Let us start by noting that all 2HDM are protected against charge and CP-breaking [35]. From the requirement of perturbativity for the top and bottom Yukawa couplings [24], $\tan\beta$ is constrained to lie

in the range $0.3 \leq \tan \beta \leq 100$. The Higgs potential is also constrained from the tree-level perturbativity and vacuum stability constraints on λ_i [36]. These are particularly interesting constraints, because they prove to be very restrictive giving us valuable information on the allowed range of the parameter space. In general terms, perturbativity arguments force $\tan \beta$ to be less than 10, but we will restrain ourselves to smaller values of $\tan \beta$ except for the case of the fermiophobic limit. Note however that all values presented in the plots are consistent with all theoretical and experimental bounds described in this section.

III. $\gamma\gamma \rightarrow S_i S_j$, $S_{i,j} = h^0, H^0, A^0$ IN THE 2HDM

A. About the one-loop calculation

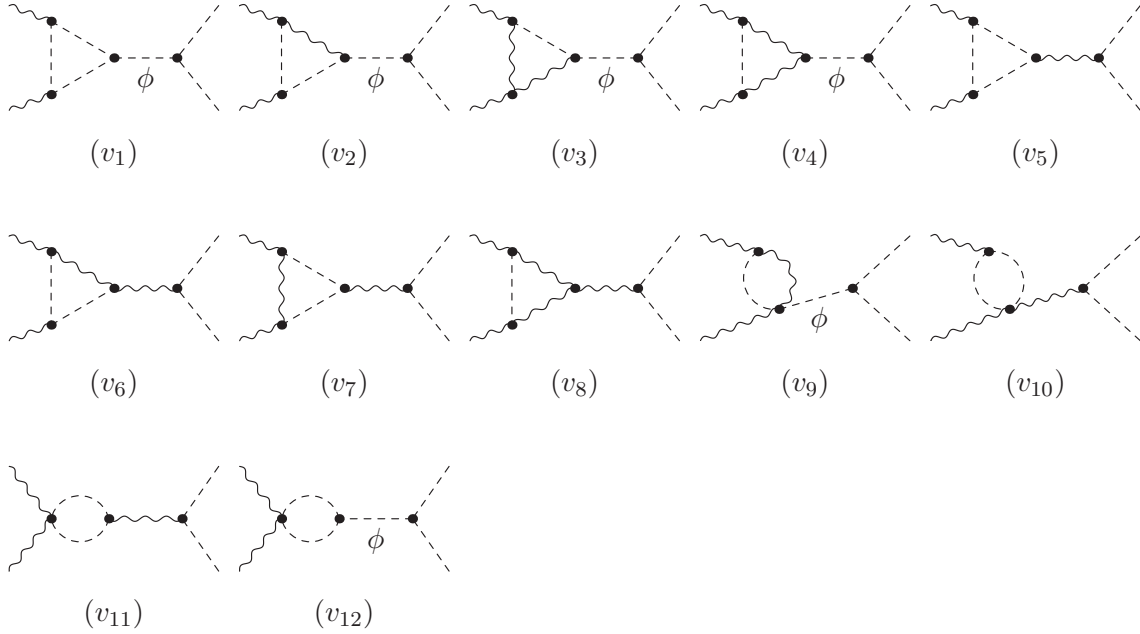


FIG. 1: Generic charged Higgs and gauge bosons vertex Feynman diagrams for neutral Higgs production $\gamma\gamma \rightarrow S_i S_j$ in 2HDM.

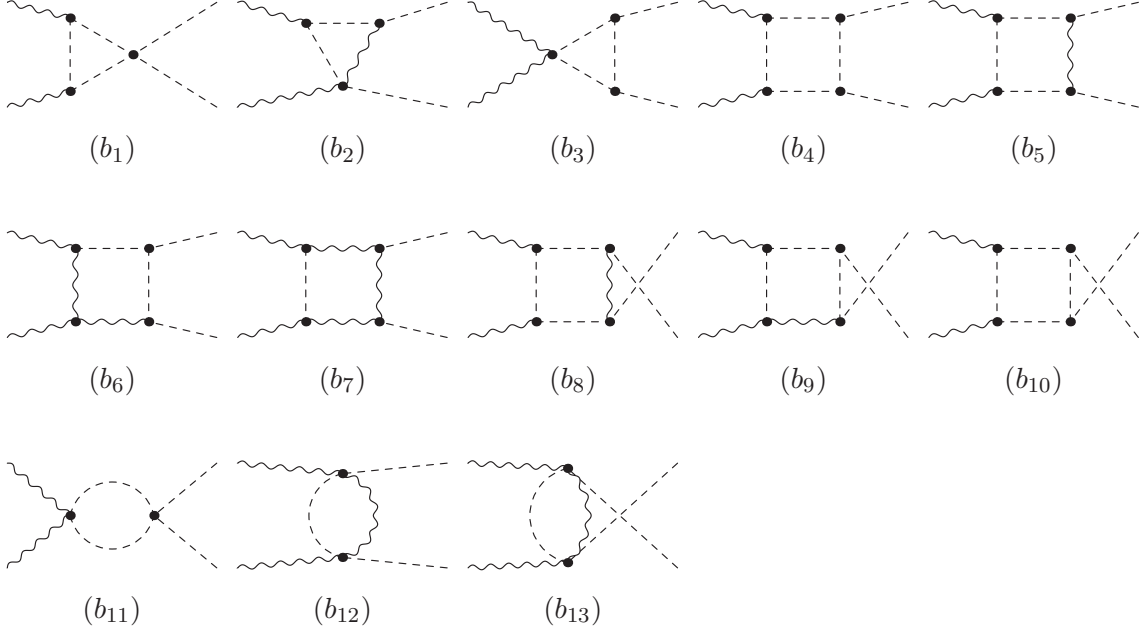


FIG. 2: Generic charged Higgs and gauge bosons box Feynman diagrams to neutral Higgs production $\gamma\gamma \rightarrow S_i S_j$ in 2HDM.

All processes $\gamma\gamma \rightarrow S_i S_j$, $S_{i,j} = h^0, H^0, A^0$ with neutral Higgs in the final state are forbidden at tree-level and are mediated at one-loop level by vertex diagrams as well as by box diagrams. All those processes are sensitive to virtual gauge bosons, fermions and charged Higgs particles. We display in Fig. 1 and in Fig. 2 the generic Feynman diagrams with charged scalar particles exchange that contribute to $\gamma\gamma \rightarrow S_i S_j$ processes. Note that in Fig. 1 and in Fig. 2 we do not show the SM contribution with fermions and gauge bosons exchange. We have checked that they are always negligible when compared to diagrams with scalar exchange. The later comprise one-loop photon-photon fusion diagrams resulting in $\phi = h^0$ or H^0 intermediate states, followed by the decay $h^0, H^0 \rightarrow S_i S_j$ with $S_{i,j} = h^0, A^0$ as shown in Fig. 1, $v_{1 \rightarrow 4}$, v_9 and v_{12} . This kind of topology is sensitive to the triple Higgs couplings $h^0 S_i S_j$, $H^0 S_i S_j$, $h^0 H^+ H^-$ and $H^0 H^+ H^-$. For the $\gamma\gamma \rightarrow h^0 A^0$ process, we have diagrams like $v_{1 \rightarrow 4}$, v_9 and v_{12} but with $\phi = A^0$ and also the contribution from the vertices with s-channel exchange of a Z boson $v_{5 \rightarrow 8}$, v_{10} and v_{11} . Note that for topologies like $v_{1 \rightarrow 4}$, v_9 and v_{12} in Fig. 1 we have included the total width of the scalar particle ϕ in the calculation of the corresponding amplitude.

For the production mode $\gamma\gamma \rightarrow h^0 h^0$, the box contributions with virtual charged Higgs

exchange is sensitive to the triple Higgs coupling $h^0 H^+ H^-$. On the contrary, in the case of the $\gamma\gamma \rightarrow A^0 A^0$ process and again due to the CP nature of the pseudo-scalar Higgs boson A^0 , it turns out that the box diagrams for $\gamma\gamma \rightarrow A^0 A^0$ are rather sensitive to the $A^0 H^+ G^-$ coupling which does not have neither a m_{12} nor a $\tan\beta$ dependence. As one can see from Fig. 2 (diagrams (b_1) and (b_{11})), there are other topologies that contribute to $\gamma\gamma \rightarrow h^0 h^0$ and $\gamma\gamma \rightarrow A^0 A^0$ and which are sensitive to quartic couplings of the Higgs boson such as $h^0 h^0 H^+ H^-$ and $A^0 A^0 H^+ H^-$.

As stated before, we are mainly concerned with the production modes $\gamma\gamma \rightarrow h^0 h^0$ and $\gamma\gamma \rightarrow A^0 A^0$. We will briefly comment on the $h^0 A^0$, $H^0 A^0$, $h^0 H^0$ and $H^0 H^0$ production processes. The one-loop amplitudes were generated and calculated with the packages FeynArts [37] and FormCalc [38]. The scalar integrals were evaluated with LoopTools [39]. The numerical evaluations of the integration over $2 \rightarrow 2$ phase space is done by the help of CUBA library [40]. A cut of approximately 6° relative to the beam axis was set on the scattering angle in the forward and backward directions.

B. Triple Higgs couplings

The above processes are sensitive to triple and quartic Higgs couplings. Below, we list the relevant pure scalar couplings needed for our processes $\gamma\gamma \rightarrow h^0 h^0, A^0 A^0, h^0 A^0$. In the SM and in the general 2HDM these triple and quartic scalar couplings are given at tree-level by

$$\lambda_{h^0 h^0 h^0}^{SM} = \frac{-3gm_{h^0}^2}{2m_W} \quad , \quad \lambda_{h^0 h^0 h^0 h^0}^{SM} = \frac{-3g^2 m_{h^0}^2}{4m_W^2} \quad (3)$$

$$\lambda_{h^0 h^0 h^0}^{2HDM} = \frac{-3g}{m_W s_{2\beta}^2} \left[(c_\beta c_\alpha^3 - s_\beta s_\alpha^3) s_{2\beta} m_{h^0}^2 - c_{\beta-\alpha}^2 c_{\beta+\alpha} m_{12}^2 \right] \quad (4)$$

$$\lambda_{H^0 H^0 H^0}^{2HDM} = \frac{-3g}{m_W s_{2\beta}^2} \left[(c_\beta c_\alpha^3 - s_\beta s_\alpha^3) s_{2\beta} m_{H^0}^2 - s_{\beta-\alpha}^2 s_{\beta+\alpha} m_{12}^2 \right] \quad (5)$$

$$\lambda_{H^0 h^0 h^0}^{2HDM} = -\frac{1}{2} \frac{g c_{\beta-\alpha}}{s_W s_{2\beta}^2} \left[(2m_{h^0}^2 + m_{H^0}^2) s_{2\alpha} s_{2\beta} - (3s_{2\alpha} - s_{2\beta}) m_{12}^2 \right] \quad (6)$$

$$\lambda_{H^0 H^0 h^0}^{2HDM} = \frac{1}{2} \frac{g s_{\beta-\alpha}}{m_W s_{2\beta}^2} \left[(m_{h^0}^2 + 2m_{H^0}^2) s_{2\alpha} s_{2\beta} - (3s_{2\alpha} + s_{2\beta}) m_{12}^2 \right] \quad (7)$$

$$\lambda_{A^0 A^0 h^0}^{2HDM} = \frac{-g}{m_W s_{2\beta}^2} \left[(c_\alpha c_\beta^3 - s_\alpha s_\beta^3) s_{2\beta} m_{h^0}^2 - c_{\beta+\alpha} m_{12}^2 + s_{2\beta}^2 s_{\beta-\alpha} m_{A^0}^2 \right] \quad (8)$$

$$\lambda_{A^0 A^0 H^0}^{2HDM} = \frac{-g}{m_W s_{2\beta}^2} \left[(s_\alpha c_\beta^3 + c_\alpha s_\beta^3) s_{2\beta} m_{H^0}^2 - s_{\beta+\alpha} m_{12}^2 + s_{2\beta}^2 c_{\beta-\alpha} m_{A^0}^2 \right] \quad (9)$$

$$\lambda_{A^0 G^0 h^0}^{2HDM} = \frac{1}{2} \frac{g c_{\beta-\alpha}}{m_W} (m_{A^0}^2 - m_{h^0}^2) \quad , \quad \lambda_{A^0 G^0 H^0}^{2HDM} = -\frac{1}{2} \frac{g s_{\beta-\alpha}}{m_W} (m_{A^0}^2 - m_{H^0}^2) \quad (10)$$

$$\lambda_{H^\pm H^\mp h^0}^{2HDM} = \frac{g}{m_W s_{2\beta}} \left[(s_\alpha s_\beta^3 - c_\alpha c_\beta^3) s_{2\beta} m_{h^0}^2 + c_{\beta+\alpha} m_{12}^2 - s_{2\beta}^2 s_{\beta-\alpha} m_{H^\pm}^2 \right] \quad (11)$$

$$\lambda_{H^\pm H^\mp H^0}^{2HDM} = \frac{-g}{m_W s_{2\beta}} \left[(s_\alpha c_\beta^3 + s_\alpha s_\beta^3) s_{2\beta} m_{H^0}^2 - s_{\beta+\alpha} m_{12}^2 + s_{2\beta}^2 c_{\beta-\alpha} m_{H^\pm}^2 \right] \quad (12)$$

$$\begin{aligned} \lambda_{h^0 h^0 H^- H^+}^{2HDM} = & - \left(\frac{g}{2m_W s_{2\beta}} \right)^2 \left[2m_{H^\pm}^2 s_{2\beta}^2 s_{\beta-\alpha}^2 + m_{h^0}^2 (2c_{\alpha+\beta} + s_{2\alpha} s_{\beta-\alpha}) (2c_{\alpha+\beta} - s_{2\beta} s_{\beta-\alpha}) \right. \\ & \left. - c_{\beta-\alpha} s_{2\alpha} (c_{\beta-\alpha} s_{2\beta} - 2s_{\alpha+\beta}) m_{H^0}^2 - m_{12}^2 (c_{\alpha+\beta}^2 + c_{2\beta}^2 c_{\beta-\alpha}^2) \right]. \end{aligned} \quad (13)$$

$$\begin{aligned} \lambda_{A^0 A^0 H^- H^+}^{2HDM} = & - \left(\frac{g}{2m_W s_{2\beta}} \right)^2 \left[m_{H^0}^2 (c_{\beta-\alpha} s_{2\beta} - 2s_{\beta+\alpha})^2 + m_{h^0}^2 (2c_{\beta+\alpha} - s_{2\beta} s_{\beta-\alpha})^2 \right. \\ & \left. - 2m_{12}^2 c_{2\beta}^2 \right] \end{aligned} \quad (14)$$

where $g = e/\sin\theta_W$ is the $SU(2)_L$ gauge coupling constant. Here we use the short-hand notations s_θ and c_θ to denote, respectively, $\sin\theta$ and $\cos\theta$ where θ stands for α or β . All these triple Higgs couplings have a strong dependence on the physical masses m_ϕ ($\phi = h^0, H^0, H^\pm, A^0$), on the mixing angles α and β and finally on the m_{12} parameter which parameterizes the soft breaking of Z_2 symmetry.

IV. NUMERICAL RESULTS

A. The general 2HDM

Before discussing our numerical results, it is worth pointing out that the following results are valid for all Yukawa type of couplings that do not generate FCNC at tree-level, as long as $\tan\beta$ remains small ($\tan\beta \lesssim 7$). Moreover, as we will see later, the 2HDM contribution is dominated by scalar loops rather than by fermion loops and the former are not model dependent. Since data can easily accommodate light h^0 and A^0 scalars [20] in the 2HDM, we will concentrate hereafter on the $h^0 h^0$, $A^0 A^0$ and $h^0 A^0$ production modes.

We first note that we have reproduced the SM result for $\gamma\gamma \rightarrow H^0 H^0$ and found perfect agreement with [12, 13]. In Fig. 3, we have performed a comprehensive scan of the parameter space of the 2HDM looking for regions where the 2HDM dominate over the SM, that is, $\sigma_{2HDM}(\gamma\gamma \rightarrow h^0 h^0) > \sigma_{SM}(\gamma\gamma \rightarrow h^0 h^0)$, together with perturbativity and vacuum stability constraints on λ_i . It is clear that in order to have a 2HDM cross section for $\gamma\gamma \rightarrow h^0 h^0$ larger than the corresponding SM one, a light charged Higgs together with a small value for

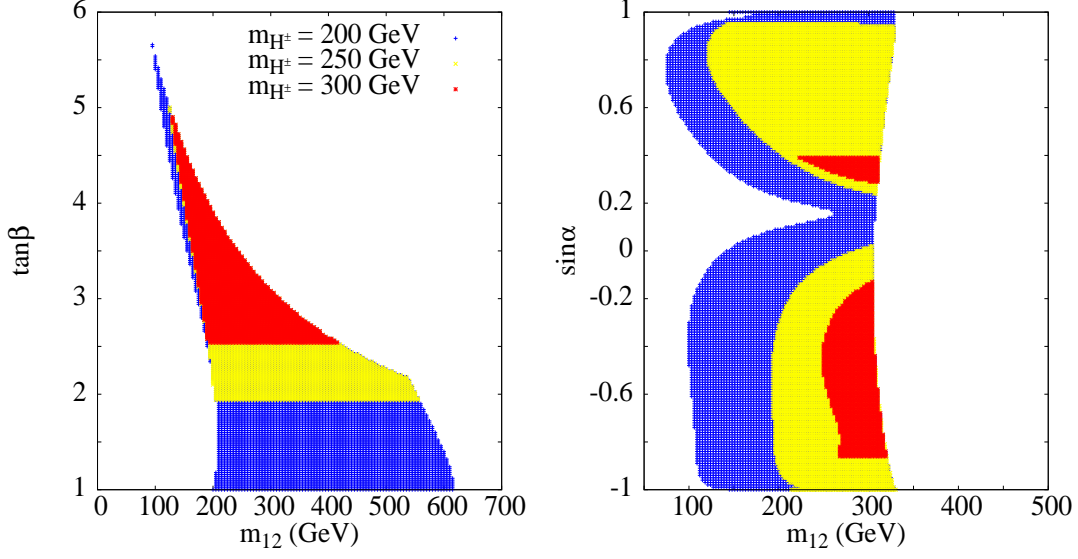


FIG. 3: The allowed region on the $(m_{12} - \tan\beta)$ plane (left) and on the $(m_{12} - \sin\alpha)$ plane (right), taking into account the perturbativity and vacuum stability constraints and asking that $\sigma_{2HDM}(\gamma\gamma \rightarrow h^0 h^0) > \sigma_{SM}(\gamma\gamma \rightarrow h^0 h^0)$ for three different values of m_{H^\pm} and for fixed $m_{h^0} = 120$ GeV, $m_{H^0} = 240$ GeV and $m_{A^0} = 100$ GeV. In the left panel $\sin\alpha = 0.5$ and in the right panel $\tan\beta = 3$.

$\tan\beta$ would be required. One can also see from the left scan that as $\tan\beta$ grows larger and larger, only smaller values of m_{12} are allowed. From the right plot in Fig. 3 one can see that negative values of $\sin\alpha$ are slightly preferred. Note that the triple and quartic couplings depend strongly on $\sin\alpha$ and $\tan\beta$. A variation of $\sin\alpha$ from $[-1, 1]$ can force some trilinear couplings $h^0 H^+ H^-$, $H^0 H^+ H^-$, $h^0 h^0 h^0$, etc., to vanish for some specific value of $\sin\alpha$ which consequently suppresses the cross section. For growing charged Higgs mass, the positive region of $\sin\alpha$ shrinks and almost disappears for a 300 GeV charged Higgs mass. However, it is clear from the scans presented that for a relatively light charged Higgs boson we have a significant slice of the parameter space where $\sigma_{2HDM}(\gamma\gamma \rightarrow h^0 h^0)$ can be larger than the corresponding SM cross section while complying with all constraints both experimental and theoretical.

In Fig. 4 (left) we show the unpolarized cross section for $\gamma\gamma \rightarrow h^0 h^0$ both in the SM and in the 2HDM. For a clear understanding of the weight of the various contributions to this process we have decided to show not only the total 2HDM and SM cross sections but also

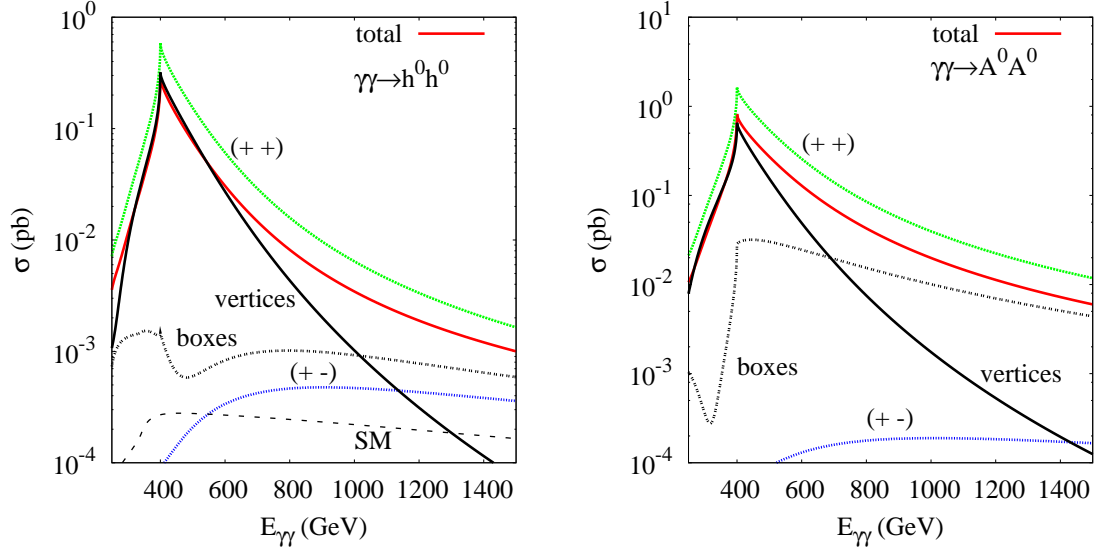


FIG. 4: SM, 2HDM vertices, 2HDM boxes and 2HDM total cross sections $\sigma(\gamma\gamma \rightarrow h^0 h^0)$ (left) and $\sigma(\gamma\gamma \rightarrow A^0 A^0)$ (right) as a function of the two photon center-of-mass energy for unpolarized beams. Also shown is the total cross section two other situations: both beams with right polarization and the two beams with opposite polarization. The parameters are chosen to be $m_{h^0}, m_{H^0}, m_{A^0}, m_{H^\pm} = 120, 240, 100, 200 \text{ GeV}$, $\sin \alpha = 0.5$, $\tan \beta = 3$, $m_{12} = 300 \text{ GeV}$.

the separate 2HDM box and the 2HDM vertex contributions. It is clear from the plot that the vertex contribution is the most important for $E_{\gamma\gamma} \lesssim 1000 \text{ GeV}$. This vertex contribution is amplified by the threshold effect when $E_{\gamma\gamma} \approx 2m_{H^\pm} = 400 \text{ GeV}$, corresponding to the opening of the charged Higgs pair channel, $\gamma\gamma \rightarrow H^+ H^-$. Near this threshold region, the cross section of the 2HDM is about three times larger than SM one. Note however that the relative weight of the different contributions depend on the parameters of the model and in particular on the value of $\sin \alpha$. Let us take $h^0 h^0$ production as an example. The value of the couplings for this set of parameters is

$$\begin{aligned}
 \lambda_{h^0 H^+ H^-}^{2HDM} &\approx \lambda_{h^0 A^0 A^0}^{2HDM} \approx 4 \times \lambda_{h^0 h^0 h^0}^{SM} \\
 \lambda_{H^0 h^0 h^0}^{2HDM} &\approx 20 \times \lambda_{h^0 h^0 h^0}^{SM} \\
 \lambda_{H^0 H^+ H^-}^{2HDM} &\approx \lambda_{H^0 A^0 A^0}^{2HDM} \approx 28 \times \lambda_{h^0 h^0 h^0}^{SM} \\
 \lambda_{h^0 h^0 h^0}^{2HDM} &\approx 8 \times \lambda_{h^0 h^0 h^0}^{SM} \\
 \lambda_{h^0 h^0 H^+ H^-}^{2HDM} &\approx \lambda_{A^0 A^0 H^+ H^-}^{2HDM} \approx 20 \times \lambda_{h^0 h^0 h^0}^{SM} .
 \end{aligned} \tag{15}$$

Now the largest contribution to the triangle comes from the vertices $H^0 H^+ H^-$ and $H^0 h^0 h^0$ which in total is approximately 560 times larger than $(\lambda_{h^0 h^0 h^0}^{SM})^2$. The larger box contribution has either the quartic vertex $h^0 h^0 H^+ H^-$ or twice the triple vertex $h^0 H^+ H^-$; whatever the situation is, the box contribution is always below 20 times $(\lambda_{h^0 h^0 h^0}^{SM})^2$. We will see later that by changing the value of $\sin \alpha$ the box contribution can be the dominant one.

In the right panel of Fig. 4 the CP-odd Higgs boson pair production $\gamma\gamma \rightarrow A^0 A^0$ is shown. Again, we present separately the vertex, boxes and the total 2HDM cross sections. The conclusions are very similar to the ones for the $h^0 h^0$ final state. In both cases, the total cross sections for $\gamma\gamma \rightarrow h^0 h^0$ and $\gamma\gamma \rightarrow A^0 A^0$ is dominated by vertex contributions for $E_{\gamma\gamma} \lesssim 1000 \text{ GeV}$ and $E_{\gamma\gamma} \lesssim 700 \text{ GeV}$ respectively. This dominance is amplified by the threshold effect when $E_{\gamma\gamma} \approx 2m_{H^\pm}$. It is also interesting to note that for high center of mass energies $E_{\gamma\gamma} \gtrsim 700 \text{ GeV}$, the box contributions start to compete with the vertex contributions. This is somehow expected since boxes have those t and u channel topologies which are enhanced for large center of mass energies. There are however no differences due to the different CP-nature in the two cross sections - not only they have the same global behavior but also very similar magnitudes. We have repeated the calculation for larger values of the A^0 mass to find a sharp fall of the cross section with increasing pseudo-scalar mass.

In Fig. 4, we also show that when the initial photons are both right handed ($++$) or left handed ($--$) polarized, the cross sections are slightly enhanced by a factor of two. In the opposite case, when the initial photons have different polarizations, right handed and left handed ($+-$) or left handed and right handed ($-+$), the cross sections are suppressed compared to unpolarized case.

In Fig. 5 we present the total cross section for $\gamma\gamma \rightarrow h^0 h^0$ (left) and $\gamma\gamma \rightarrow A^0 A^0$ (right) as a function of the two photon center of mass energy for different values of the charged Higgs mass. In both cases the cross sections are enhanced in the region of threshold where $E_{\gamma\gamma} \approx 2m_{H^\pm}$ and can reach a few pico-barn. For this specific scenario of $\sin \alpha = -0.86$, we note that the trilinear and quartic couplings have the following size as compared to the SM $\lambda_{h^0 h^0 h^0}^{SM}$ and $\lambda_{h^0 h^0 h^0 h^0}^{SM}$:

$$\begin{aligned}\lambda_{h^0 H^+ H^-}^{2HDM} &\approx \lambda_{h^0 A^0 A^0}^{2HDM} = \lambda_{H^0 h^0 h^0}^{2HDM} \approx 25 \times \lambda_{h^0 h^0 h^0}^{SM} \\ \lambda_{H^0 H^+ H^-}^{2HDM} &\approx \lambda_{H^0 A^0 A^0}^{2HDM} \approx 5 \times \lambda_{h^0 h^0 h^0}^{SM}\end{aligned}$$

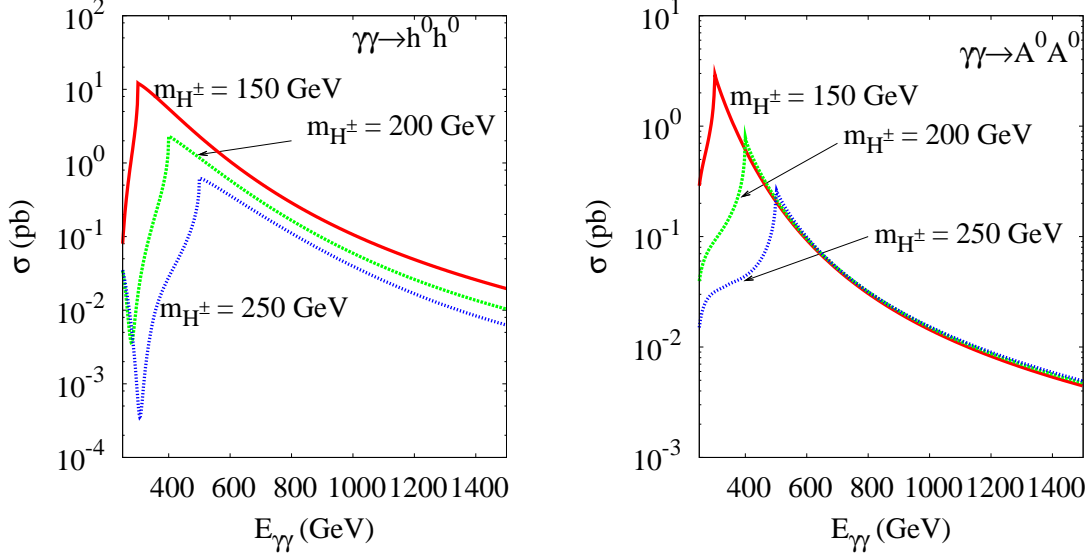


FIG. 5: The total cross section of $\sigma(\gamma\gamma \rightarrow h^0 h^0)$ (left) and $\sigma(\gamma\gamma \rightarrow A^0 A^0)$ (right) as a function of two photon center-of-mass energy $E_{\gamma\gamma}$ in the 2HDM. With $m_{h^0}, m_{H^0}, m_{A^0}, m_{12} = 120, 200, 120, 300$ GeV, $\sin \alpha = -0.86$ and $\tan \beta = 3$ for different values of m_{H^\pm} .

$$\begin{aligned}\lambda_{h^0 h^0 h^0}^{2HDM} &\approx 40 \times \lambda_{h^0 h^0 h^0}^{SM} \\ \lambda_{h^0 h^0 H^+ H^-}^{2HDM} &\approx \lambda_{A^0 A^0 H^+ H^-}^{2HDM} \approx 55 \times \lambda_{h^0 h^0 h^0}^{SM}\end{aligned}\quad (16)$$

As a consequence, in the case of the $\gamma\gamma \rightarrow h^0 h^0$ mode, the total cross section is now fully dominated by box contributions both at low and high energies. In the case of $\gamma\gamma \rightarrow A^0 A^0$ mode, the situation is slightly different. For low energy $E_{\gamma\gamma} \lesssim 780$ GeV, the total cross section is dominated by vertex while for high energies $E_{\gamma\gamma} \gtrsim 780$ GeV, it is dominated by the box contributions. In addition, we note that there is a destructive interference between box and vertex contributions for low energies. We conclude that at high energies, both for the $\gamma\gamma \rightarrow h^0 h^0$ and for the $\gamma\gamma \rightarrow A^0 A^0$ modes, the total contribution is dominated by boxes and that is why at $E_{\gamma\gamma} = 1.5$ TeV the cross section is still of the order 0.01 pb.

In Fig. 6 we show the total cross section for $\gamma\gamma \rightarrow h^0 h^0$ (left) and $\gamma\gamma \rightarrow A^0 A^0$ (right) as a function the heavy Higgs mass for several values of the two photon center of mass energy. The threshold effect when $E_{\gamma\gamma} \approx 2m_{H^\pm}$ is again seen in both plots. Both figures show another very important feature, the strong dependence of the cross section on vertex diagrams with an intermediate heavy Higgs (virtual or not) that then decays to $h^0 h^0$ or $A^0 A^0$. That is why we have exactly the same threshold effects in both plots. The width

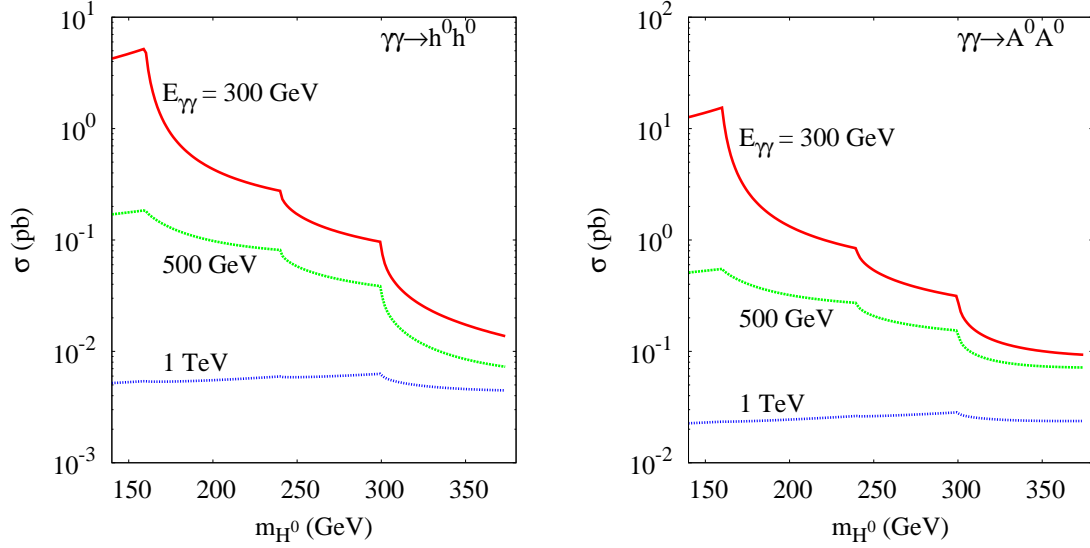


FIG. 6: The total cross section of $\sigma(\gamma\gamma \rightarrow h^0 h^0)$ (left) and $\sigma(\gamma\gamma \rightarrow A^0 A^0)$ (right) as a function of the heavy Higgs mass m_{H^0} in the 2HDM. With $m_{h^0}, m_{H^\pm}, m_{A^0}, m_{12} = 120, 150, 80, 400 \text{ GeV}$, $\sin \alpha = 0.5$ and $\tan \beta = 2.5$ for different values of the two photon center-of-mass energy $E_{\gamma\gamma}$.

in the propagator changes every time a new channel opens. The first bump in the plots is due to the opening of the $H^0 \rightarrow W^+ W^-$ and $H^0 \rightarrow A^0 A^0$ channels. The second bump is due to the opening of $H^0 \rightarrow h^0 h^0$ near 240 GeV and the third one is close to 300 GeV where the $H^0 \rightarrow H^+ H^-$ starts to be kinematically allowed. Therefore, we conclude that a lighter heavy Higgs, which is at least below the $2 M_W$ threshold, will allow a much easier characterization of Higgs potential.

In the case of $h^0 A^0$ or $H^0 A^0$ final state, the situation is different. Due to the presence of the CP odd scalar A^0 in the final state, the Higgs boson ϕ in the s-channel vertex (Fig. 1) $v_{1 \rightarrow 4}, v_9$ and v_{12} must also be CP-odd. Hence, the processes $\gamma\gamma \rightarrow h^0 A^0, H^0 A^0$ do not proceed through an intermediate heavy Higgs. This implies that we will now have a dependence on the pseudo-scalar width but not on the heavy Higgs width. Note also that there is no closed loop of virtual exchange of charged Higgs or gauge bosons. We have rather a mixture of charged Higgs and charged Goldstones in the loop. We have checked that the values of the cross section of $\gamma\gamma \rightarrow h^0 A^0$ is much smaller than the $h^0 h^0$ and $A^0 A^0$ ones. This substantiates the conclusion about the importance of diagrams with a virtual H^0 . We have performed a systematic scan over the 2HDM parameters with $m_{h^0} = m_{A^0}$ in the range 100 to 160 GeV ,

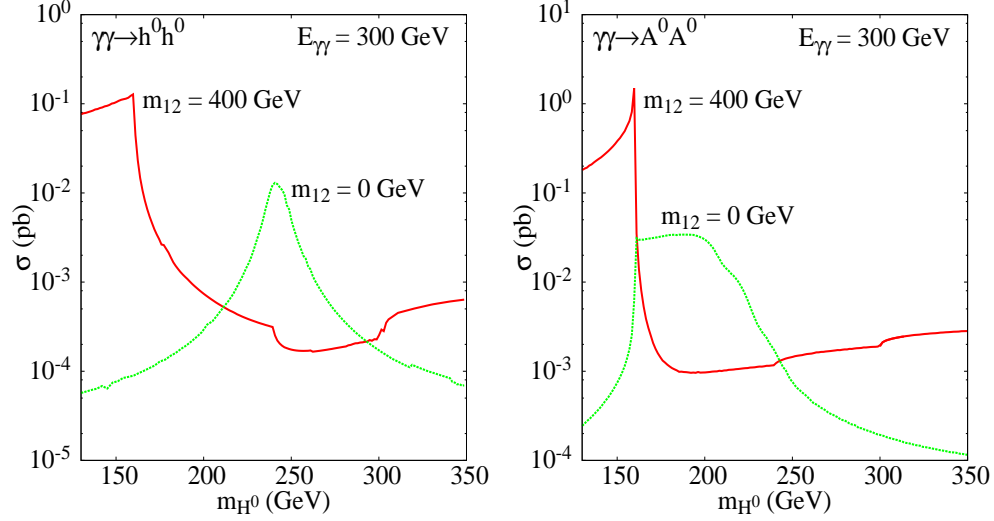


FIG. 7: The total cross section of $\sigma(e^+e^- \rightarrow \gamma\gamma \rightarrow h^0 h^0)$ (left) and $\sigma(e^+e^- \rightarrow \gamma\gamma \rightarrow A^0 A^0)$ (right) as a function of the heavy Higgs mass m_{H^0} in the 2HDM for $E_{\gamma\gamma} = 300 \text{ GeV}$. With $m_{h^0} = 120 \text{ GeV}$, $m_{H^\pm} = 150$, $m_{A^0} = 80 \text{ GeV}$, $\sin \alpha = 0.5$, $\tan \beta = 2.5$ for two values of m_{12} .

and found that the cross section of $\gamma\gamma \rightarrow h^0 A^0$ can not exceed 0.2 pb . We found that large cross section for $\gamma\gamma \rightarrow h^0 A^0$ prefer rather small values of $\tan \beta \lesssim 3$, $|\sin \alpha| \gtrsim 0.5$, $m_{12} \gtrsim 450 \text{ GeV}$ and also low center of mass energies $\sqrt{s} \lesssim 600 \text{ GeV}$.

Regarding the production modes $\gamma\gamma \rightarrow h^0 H^0$ and $\gamma\gamma \rightarrow H^0 H^0$ we note that they are obviously phase space suppressed due to the heavier Higgs in the final state and because there is no significant difference in the contributing diagrams, their total cross section is necessarily smaller than the $h^0 h^0$ and $A^0 A^0$ ones.

Finally, in Fig. 7 we show the total cross section for $e^+e^- \rightarrow \gamma\gamma \rightarrow h^0 h^0$ (left) and for $e^+e^- \rightarrow \gamma\gamma \rightarrow A^0 A^0$ (right) as a function the heavy Higgs mass for two values of m_{12} . The total cross section for this Figure is evaluated by convoluting the photon-photon cross section with the photon-photon luminosity spectrum taken from the CompAZ library [41]. CompAZ is based on formulae for the Compton scattering and provides the photon energy spectrum for different beam energies and the average photon polarization for a given photon energy.

First, let us remark that again this cross section is large enough to be measured in a significant region of the parameter space. We can still see the heavy Higgs width effects but somehow softened by the photon spectrum. The more interesting region is still the one

where $m_{H^0} \leq 2m_W$ and m_{12} is large where the cross section can reach the pico-barn level. For $m_{12} = 0 \text{ GeV}$ the cross section for $e^+e^- \rightarrow \gamma\gamma \rightarrow h^0h^0$ peaks at around $2m_{h^0}$ with a value of $\approx 10 \text{ fb}$.

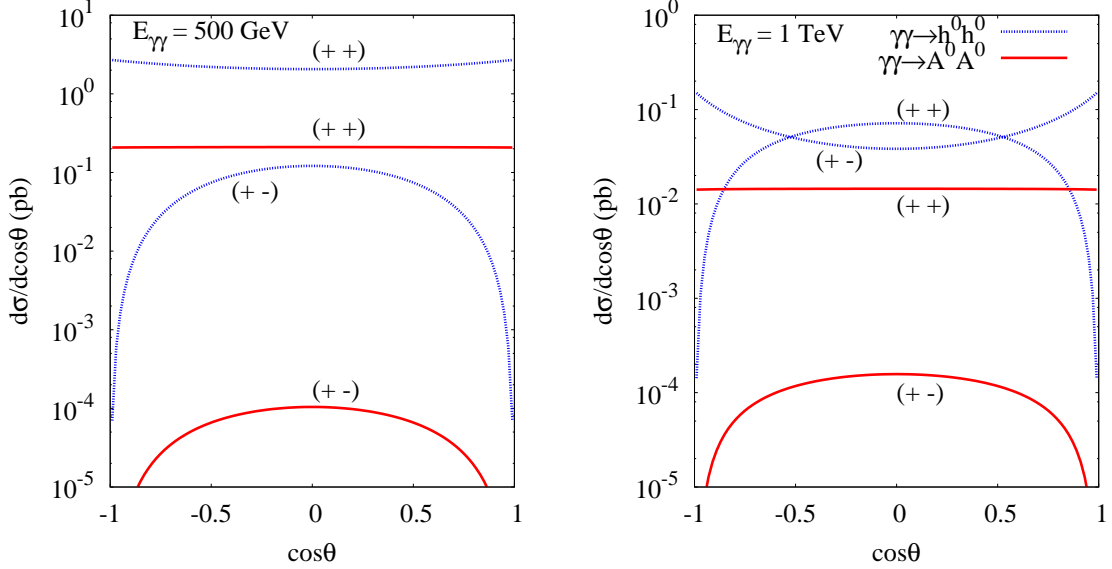


FIG. 8: The differential cross sections for $\gamma\gamma \rightarrow h^0h^0$ and $\gamma\gamma \rightarrow A^0A^0$ with right handed polarized photons (+) and left handed polarized photons (-) for $\sqrt{s} = 500 \text{ GeV}$ (left) and $\sqrt{s} = 1000 \text{ GeV}$ (left). The 2HDM parameters are the same as in Fig. 5 and $m_{H\pm}$ fixed at 150 GeV .

Let us now turn to the differential cross section for $\gamma\gamma \rightarrow h^0h^0$ and $\gamma\gamma \rightarrow A^0A^0$. In Fig. 8 we illustrate the differential cross for a center of mass energy of $\sqrt{s} = 500 \text{ GeV}$ and $\sqrt{s} = 1 \text{ TeV}$ and for identically polarized $(++)$, $(--)$ and oppositely polarized $(+-)$, $(-+)$ initial photons. As one can see from left panel for $\sqrt{s} = 500 \text{ GeV}$, for both the h^0h^0 and the A^0A^0 modes, the angular distribution for $(++)$ and $(--)$ polarized photons is almost flat while for the $(+-)$ and $(-+)$ modes it has a parabolic shape with a rather small cross section except for $\gamma\gamma \rightarrow h^0h^0$ where in the region of $-0.5 < \cos\theta < 0.5$ the differential cross section is of the order of 0.1 pb . For $\sqrt{s} = 1 \text{ TeV}$, Fig. 8 (right panel), it is clear that for the h^0h^0 mode, the angular distributions for $(++)$ and $(+-)$ are almost flat with rather large cross sections - about 0.1 pb in the region $-0.5 < \cos\theta < 0.5$. Regarding the A^0A^0 mode, the angular distribution for $(++)$ is flat and for the $(+-)$ mode the value of the differential cross section is very small.

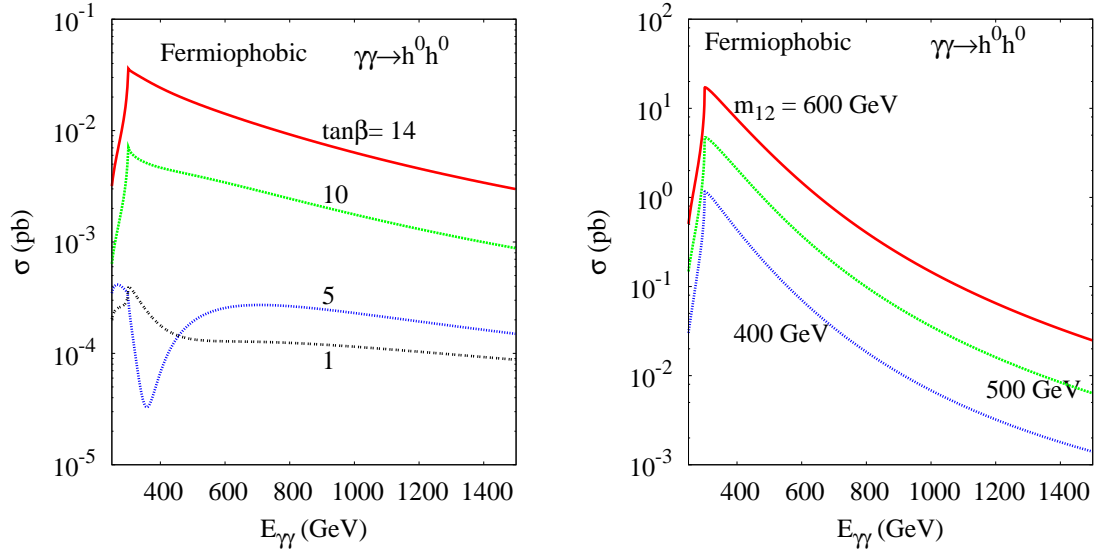


FIG. 9: The total cross section for $\gamma\gamma \rightarrow h^0 h^0$ as a function of the two photons center-of-mass energy $E_{\gamma\gamma}$ in the fermiophobic limit. In the left panel, the cross section is shown for 4 different $\tan\beta$ values and in the right panel for 3 different m_{12} values. The other parameters, if not shown are: $m_h = 120 \text{ GeV}$, $m_{H^\pm} = 150$, $m_A = 80 \text{ GeV}$, $m_H = 240 \text{ GeV}$, $m_{12} = 0 \text{ GeV}$ and $\tan\beta = 1$.

B. Fermiophobic limit

In the SM, where just one doublet couples to all fermions, each scalar couples to the different fermions with the same coupling constant. In a general 2HDM it is also possible to couple just one doublet to all fermions by choosing an appropriate symmetry for both the fermions and the scalars. However, the difference between the SM and the 2HDM is that now the couplings are proportional to the rotation angles α and β . For instance, the lightest CP-even Higgs couples to all fermions as $\cos\alpha/\sin\beta g_{hff}^{SM}$. By choosing $\alpha = \pm\pi/2$, the lightest Higgs decouples from all fermions. Such a scenario, with the appearance of the so-called "fermiophobic" Higgs boson, arise in a variety of models [26]. The heavy CP-even scalar will acquire larger couplings to the fermions than the corresponding SM couplings. All the remaining scalars are not affected by this choice as they do not couple proportionally to α .

In the situation where the Higgs-fermion couplings are substantially suppressed, the full decay width of the Higgs boson is shared mostly between the WW , ZZ and $\gamma\gamma$ decay modes. In this limit, for masses $m_{h^0} < 100 \text{ GeV}$, the Higgs boson dominantly decays to photon pairs. Experimental searches for fermiophobic Higgs bosons at the LEP collider and the Tevatron

collider have yielded negative results. Mass limits have been set in a benchmark model that assumes that the couplings hWW and hZZ have the same strength as in the SM and that all fermion branching ratios are exactly zero. Combination of the results obtained by the LEP collaborations [42, 43, 44, 45] using the process $e^+e^- \rightarrow hZ, h \rightarrow \gamma\gamma$ yielded the lower bound $m_h > 109.7 \text{ GeV}$ at 95% C.L. [46]. In Run I, Tevatron has set lower limits on m_h by the D0 and CDF collaborations which are respectively 78.5 GeV [47] and 82 GeV [48], using the processes $q\bar{q}' \rightarrow V^* \rightarrow hW, hZ, h \rightarrow \gamma\gamma$, with the dominant contribution coming from W . Recently the CDF [49] and the D0 [50] collaborations have improved their bounds which are now of the order of 100 GeV , close to the bound obtained by the LEP collaborations. It should be noted that all experimental mass bounds assume, in the fermiophobic limit, $\tan\beta \sim 0$ in the tree-level couplings to the gauge bosons.

It is clear that in the fermiophobic limit the coupling $H^0 h^0 h^0$ (Eq. (6)) is directly proportional to m_{12} , while the other couplings depend both on m_{12} , $\tan\beta$ as well as on m_{H^\pm} . Keeping the perturbativity and vacuum stability constraints as well as the $\Delta\rho$ bound, we show in Fig. 9, the total cross section for $\gamma\gamma \rightarrow h^0 h^0$ as a function of the two photon center of mass energy in the fermiophobic limit for $m_{h^0} = 120 \text{ GeV}$ and $m_{A^0} = 80 \text{ GeV}$. The other CP-even Higgs mass is taken to be $m_{H^0} = 2m_{h^0}$ such that the resonant channel $H^0 \rightarrow h^0 h^0$ is open. The other parameters are $m_{H^\pm} = 150 \text{ GeV}$, and $m_{12} = 0 \text{ GeV}$. In both cases, we plot the total cross sections for several values of $\tan\beta$. It is clear that the cross section is enhanced for large $\tan\beta$. This region is complementary to one probed at LEP where $\tan\beta$ was very small. The observed kink around $E_{\gamma\gamma} = 2m_{H^\pm} = 300 \text{ GeV}$, in the left and right panels, is again due to the same threshold effect. In the right panel we plot the cross section for three representative values of $m_{12} = 400, 500$ and 600 GeV . It is clear that an increase in m_{12} will increase the cross section by about 3 times near the threshold region.

C. Decoupling limit

A study of 2HDM in the decoupling limit reveals the case where all scalar masses except one formally become large and the effective theory is just the SM with one doublet - $m_{h^0} \ll m_\Phi$ where $m_\Phi = m_{H^0, A^0, H^\pm}$ (see [27] for an overview). In this case, the CP-even h^0 is the lightest scalar particle while the other Higgs particles H^0, A^0 and H^\pm are extremely heavy. In 2HDM, the decoupling limit can be achieved by taking the limit $\alpha \rightarrow \beta - \pi/2$. This

means that the coupling of the h^0 to the gauge bosons, fermions and light Higgs, h^0 are the same as for the Standard Model h^{SM} Higgs. Also, in the decoupling limit, the triple Higgs coupling $\lambda_{h^0 h^0 H^0}^{(0)}$ vanishes at tree-level, so that the heavy Higgs cannot contribute to the process $\gamma\gamma \rightarrow h^0 h^0$ and the result is independent of the mass m_{H^0} . In the decoupling limit, the tree-level trilinear Higgs couplings take the form

$$\lambda_{h^0 h^0 h^0}^{2HDM} \approx \lambda_{h^0 h^0 h^0}^{SM}, \quad (17)$$

$$\lambda_{h^0 h^0 H^0}^{2HDM} \approx 0,$$

$$\lambda_{h^0 H^+ H^-}^{2HDM} \approx -\frac{g}{2m_W} \left[m_{h^0}^2 + 2m_{H^\pm}^2 - m_{12}^2 \right],$$

$$\lambda_{h^0 h^0 H^+ H^-}^{2HDM} \approx \frac{g}{2m_W} \lambda_{h^0 H^+ H^-}^{2HDM}. \quad (18)$$

It is clear that these couplings are independent of $\tan\beta$ as well. The enhancement of the cross section essentially depends on the size of the $h^0 H^+ H^-$ and $H^0 H^- H^+$ couplings. By taking these couplings as large as possible under the requirement of validity of perturbation theory, vacuum stability and also under all experimental constraints, we obtain the best enhancement of the cross section of $\gamma\gamma \rightarrow h^0 h^0$ in 2HDM for each m_Φ ($m_\Phi = m_{H^0} = m_{A^0} = m_{H^\pm}$). However, it is well known that those couplings of the CP-even h^0 which mimic the SM couplings get significant radiative corrections in the decoupling limit to which we refer as non-decoupling effects. Several studies have been carried out looking for non-decoupling effects in Higgs boson decays and Higgs self-interactions. Large loop effects in $h^0 \rightarrow \gamma\gamma$, $h^0 \rightarrow \gamma Z$ and $h^0 \rightarrow b\bar{b}$ have been pointed out for the 2HDM [51, 52] and may provide indirect information on the Higgs masses and the involved triple Higgs couplings such as $\lambda_{h^0 H^+ H^-}$, $\lambda_{h^0 H^0 H^0}$, $\lambda_{h^0 A^0 A^0}$ and $\lambda_{h^0 h^0 h^0}$.

The non-decoupling contributions to the triple Higgs self-coupling $\lambda_{h^0 h^0 h^0}$ have been investigated in the 2HDM in Ref. [53], using the Feynman diagrammatic method. It has been demonstrated that the one-loop leading contributions originated from the heavy Higgs boson loops and the top quark loops to the effective $h^0 h^0 h^0$ coupling can be written as [53]

$$\begin{aligned} \lambda_{h^0 h^0 h^0}^{eff} = & \frac{3m_{h^0}^2}{v} \left\{ 1 + \frac{m_{H^0}^4}{12\pi^2 m_{h^0}^2 v^2} \left(1 - \frac{M^2}{m_{h^0}^2} \right)^3 + \frac{m_{A^0}^4}{12\pi^2 m_{h^0}^2 v^2} \left(1 - \frac{M^2}{m_{A^0}^2} \right)^3 \right. \\ & \left. + \frac{m_{H^\pm}^4}{6\pi^2 m_{h^0}^2 v^2} \left(1 - \frac{M^2}{m_{H^\pm}^2} \right)^3 - \frac{N_c m_t^4}{3\pi^2 m_{h^0}^2 v^2} + \mathcal{O} \left(\frac{p_i^2 m_\Phi^2}{m_{h^0}^2 v^2}, \frac{m_\Phi^2}{v^2}, \frac{p_i^2 m_t^2}{m_{h^0}^2 v^2}, \frac{m_t^2}{v^2} \right) \right\}, \quad (19) \end{aligned}$$

where $M = m_{12}/\sqrt{\sin\beta\cos\beta}$, m_Φ and p_i represent the mass of H^0 , A^0 or H^\pm and the momenta of external Higgs lines, respectively, N_c denotes the number of colors, and m_t is the mass of top quark. We note that in Eq. (19) m_{h^0} is the renormalized physical mass of the lightest CP-even Higgs boson h^0 . In the calculation of the $\gamma\gamma \rightarrow h^0 h^0$ cross section in the decoupling limit, we replace the $\lambda_{h^0 h^0 h^0}^{(0)}$ coupling by its effective coupling given in Eq. (19) which corresponds, in this limit, to an effective 2-loop 2HDM contribution (see Ref. [53] for a detailed discussion).

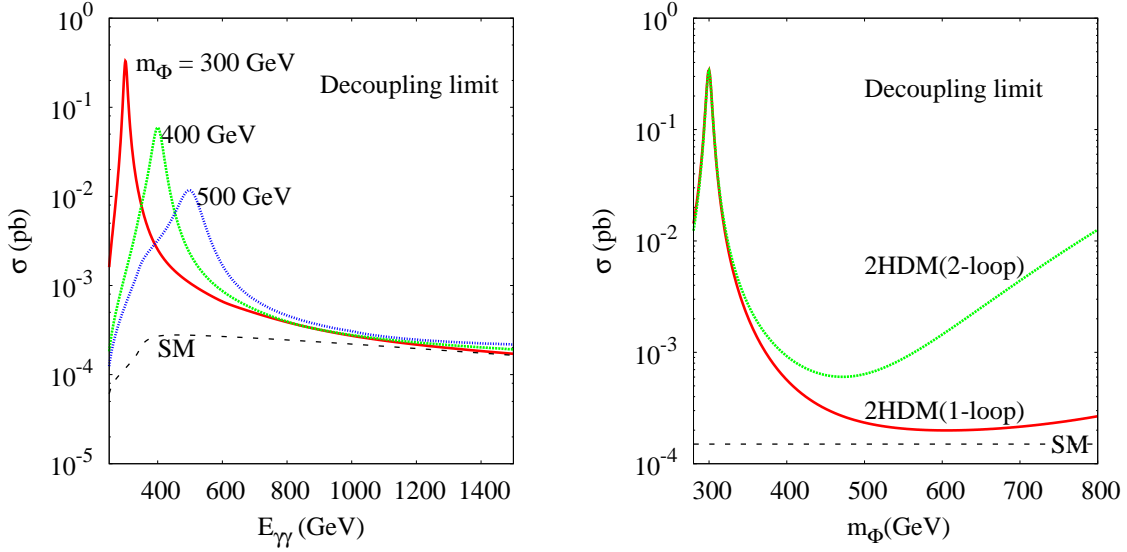


FIG. 10: Cross sections for $h^0 h^0$ production in the decoupling limit with unpolarized photons. On the right we show the loop contributions to the total cross section as a function of m_Φ with $(\sin(\beta - \alpha), \tan\beta, m_{12}) = (1, 2, 0)$. On the left panel the cross section as a function $E_{\gamma\gamma}$ is shown for different values of m_Φ and $(\sin(\beta - \alpha), \tan\beta, m_{12}) = (1, 1, 0)$. The Higgs mass is $m_{h^0} = 120$ GeV.

As stated in the introduction, this process was studied in detail in Refs. [14, 15] in the decoupling limit. In this section we just present results for the case of the unpolarized photon cross section. We show that even in this case where the cross sections would be severely reduced, there are still regions where the 2HDM h^0 could be disentangled from the SM h_{SM} . In the left panel of Fig. 10 we show the cross section of $\gamma\gamma \rightarrow h^0 h^0$ as a function of $E_{\gamma\gamma}$ for $m_\Phi = 300, 400$ and 500 GeV, in which all the other free parameters are chosen to obtain the maximal enhancement under all the constraints. In this left panel, the coupling $h^0 h^0 h^0$ is taken at the tree-level without the higher order correction of Eq.(19). At the position

near the threshold energies, the cross sections reach the maximal values 0.33 pb , 0.06 pb and 0.01 pb for $E_{\gamma\gamma} = 300 \text{ GeV}$, 400 GeV and 500 GeV respectively and after that they decrease with increasing photon-photon energy, $E_{\gamma\gamma}$. There exists a small resonant spike in the vicinity of $E_{\gamma\gamma} = 2 m_\Phi$ which implies that the effect of the charged Higgs is small. In the right panel of Fig. 10 we display the cross section of $\gamma\gamma \rightarrow h^0 h^0$ as a function m_Φ with $\sin(\beta - \alpha) = 1$, $\tan \beta = 1$ and $m_{12} = 0 \text{ GeV}$. In this right panel, we plot both cases with and without the higher order corrections given in Eq.(19). One can see that the cross section is enhanced due to the large corrections in $\lambda_{h^0 h^0 h^0}^{eff}$ which are amplified for large m_Φ . In fact, for $m_\Phi < 350 \text{ GeV}$, the cross section is enhanced by the effects of the charged Higgs loop and the top quark loop diagrams and with $m_\Phi > 350 \text{ GeV}$, the contribution of the effective coupling $\lambda_{h^0 h^0 h^0}^{eff}$ becomes important and amplifies the cross section from its SM value to a value up to two orders of magnitude higher for $m_\Phi = 800 \text{ GeV}$. It is also clear from the right panel that without the higher order corrections of Eq.(19), for large m_Φ , the 2HDM cross section is similar to SM one. On the other hand, once those high order corrections are included we can get some non decoupling effect - the cross section then grows relative to the SM one and reaches a few tens of fempto-barn for $m_\Phi = 800$, two orders of magnitude above the corresponding SM process.

V. HIGGS SIGNATURES

We are considering a light CP-even Higgs, that is, with a mass of 120 GeV or less. Assuming that all decay channels with some other Higgs boson in the final state are unaccessible, this particle decays predominantly to $b\bar{b}$ in this mass region. The exception is in the fermiophobic Higgs scenario where it decays to two photons although for a mass of 120 GeV one has already to consider the decay to two W bosons even if one of the W is off-shell and strongly virtual. The rate at which it decays to each final state depends on the remaining parameters of the 2HDM (see [54, 55] for details). The two subleading decays that compete with $h^0 \rightarrow b\bar{b}$ are $h^0 \rightarrow c\bar{c}$ and $h^0 \rightarrow \tau^+\tau^-$. In model type I the branching fractions to fermions are the SM ones because the coupling dependence cancels. In model type II, the ratio $\Gamma(h^0 \rightarrow b\bar{b})/\Gamma(h^0 \rightarrow \tau^+\tau^-)$ is the SM one. On the other hand it is easy to check that for $\tan \beta \geq 1$ the decay $h^0 \rightarrow b\bar{b}$ is again the dominant one provided we are in a region with moderate values of $\tan \alpha$. For the remaining Yukawa models the situation does

not change dramatically. However, if we take as an example the case where Φ_2 couples to the quarks and Φ_1 couples to the leptons, we obtain the ratio

$$\frac{\Gamma(h^0 \rightarrow b\bar{b})}{\Gamma(h^0 \rightarrow \tau^+\tau^-)} = \frac{m_b^2}{m_\tau^2} \frac{1}{\tan^2 \alpha \tan^2 \beta} \quad (20)$$

in the limit $m_h \gg m_q$. Even for $\tan \alpha = \tan \beta \approx 3$ the ratio becomes almost 100 times smaller than the corresponding SM ratio. Therefore, a detailed study for each model will have to take into account the exact branching fractions for each Yukawa version of the 2HDM.

The dominant background to double Higgs production is $\gamma\gamma \rightarrow W^+W^-$ which can be reduced by imposing a cut on the invariant mass of each pair of b-jets, $M(q\bar{q})$, forcing it to be close to Higgs mass. An efficient b-tagging would further reduce the background by asking that at least three jets be identified as originating from b quarks. Together they would reduce the backgrounds to a level well below the signal. A more detailed analysis can be found in [13]. In the fermiophobic case, the analysis is greatly simplified by the smallness of the four photon production cross section. We just need to avoid very soft photons which can be done with a sensible cut on the photon's transverse momentum.

The process $\gamma\gamma \rightarrow h^0 H^0$ gives rise to very similar signatures. There are in principle two drawbacks: first the phase space is reduced because there is a heavier Higgs in the final state; second we can not reduce the background by asking the two invariant masses from each pair of b-jets to have a similar magnitude. On the other hand, if the channel $H^0 \rightarrow h^0 h^0$ is open, it can be dominant. This would lead to a very interesting signal of a six b-jet final state. As for $\gamma\gamma \rightarrow h^0 A^0$ it may not suffer from phase space suppression but it is still a process where background reduction will be much harder.

A pseudo-scalar Higgs decays again mainly as $A^0 \rightarrow b\bar{b}$ and the subleading competing decays are again $A^0 \rightarrow c\bar{c}$ and $A^0 \rightarrow \tau^+\tau^-$. The situation is similar to the CP-even Higgs case - if $\tan \beta \approx 1$ the $b\bar{b}$ channel is always the dominant and well above the others. Once more if we consider the model where Φ_2 couples to the quarks and Φ_1 couples to the leptons, we obtain the ratio

$$\frac{\Gamma(A^0 \rightarrow b\bar{b})}{\Gamma(A^0 \rightarrow \tau^+\tau^-)} = \frac{m_b^2}{m_\tau^2} \frac{1}{\tan^2 \beta} \quad (21)$$

in the limit $m_h \gg m_q$. In this case, for $\tan \beta \approx 3$ the ratio becomes 10 times smaller than the corresponding SM ratio. Note that a similar situation can occur in the ratio between down and up quarks. Obviously, this is true as long as the other channels involving other

Higgs are closed. The decays to either $h^0 Z$ or $W^+ H^-$ become dominant as soon as they are kinematically allowed. The last two cases could again lead to interesting final states which are easy to detect. As all the cases discussed refer to light Higgs, even if the Higgs to Higgs channel is open the Higgs decay width will in most situation be well below the GeV or a few GeV at most.

A final word about the behavior of the cross section with the scattering angle. We have shown that if the A^0 and h^0 masses are of the same order, and because in most models the possible final states are very similar, it will be very hard to distinguish a CP-even from a CP-odd state. In fact, even if one changes the polarization of the initial photons, the differential cross section does not distinguish clearly between the two cases except in regions where either the cross sections are too small to be measured or the angle is too small to be probed.

VI. CONCLUSIONS

We have calculated the total cross section for $\gamma\gamma \rightarrow S_i S_j$, $S_i = h^0, A^0, H^0$, in the framework of the 2HDM. For the numerical study, we mainly focused on the $h^0 h^0$ and $A^0 A^0$ production modes. We have studied those processes in the general 2HDM, and in two of its particular limiting scenarios: the fermiophobic limit, a scenario where the lightest CP-even Higgs decouples from the fermions and the decoupling scenario where this same Higgs resembles the SM Higgs boson. We have shown that, for both production modes, the most important contribution to $\sigma(\gamma\gamma \rightarrow h^0 h^0)$ and to $\sigma(\gamma\gamma \rightarrow A^0 A^0)$ comes from the charged Higgs H^\pm diagrams and also from the diagrams with a resonant heavy Higgs that can decay as $H^0 \rightarrow h^0 h^0$ or $H^0 \rightarrow A^0 A^0$. The cross sections can be large in the decoupling limit but there are regions of the parameter space where they can be even larger. For instance we have witnessed an important dependence of the cross section on the angles α , $\tan\beta$ and m_{12} . We can imagine a situation where all masses are large but far from the decoupling limit due to the choice of the angles and with larger cross sections. In the decoupling limit the cross section for $h^0 h^0$ can be much larger than the corresponding SM one which may allow to disentangle 2HDM from other beyond SM models [14, 15]. In the fermiophobic limit this process is complementary to the LEP production process as it grows with $\tan\beta$. Most importantly, it can also probe a part of the parameter space that cannot be accessed

at hadron colliders. When $m_{12} \approx 0$ the cross section vanishes at hadron colliders [56]. On the contrary, we have shown that in photon-photon collisions the cross section can be quite large even for $m_{12} \approx 0$. This region of the fermiophobic scenario region will not be excluded until we have access to a photon-photon collider.

Finally we have argued that knowledge of the charged Higgs effects may be crucial to understand the nature of the Higgs bosons if they are eventually found in future experiments at LHC and/or ILC. The same is true for the heavy Higgs - a difference in its width can lead to dramatic changes in the cross section. Regarding the CP-odd Higgs, we have shown that, for the energies considered, only a light A^0 will be probed at a photon-photon collider. For $m_{A^0} \geq 150 \text{ GeV}$ the cross section is virtually zero. A last word for the final states: we have shown that in the two most popular models, 2HDM-I and 2HDM-II, the $b\bar{b}$ final state is the preferred channel as its branching fraction is always at least the SM one; in other models a detailed study has to be performed taking into account all 2HDM parameters.

VII. ACKNOWLEDGMENTS

We would like to thank the Fernando Cornet for valuable discussions. C.C.H is supported by the National Science Council of R.O.C under Grant #s: NSC-97-2112-M-006-001-MY3 and R.B is supported by National Cheng Kung University Grant No. HUA 97-03-02-063. R.S. is supported by the FP7 via a Marie Curie Intra European Fellowship, contract number PIEF-GA-2008-221707.

-
- [1] G. Weiglein *et al.* [LHC/LC Study Group], Phys. Rept. **426** (2006) 47 [arXiv:hep-ph/0410364].
 - [2] P. W. Higgs, Phys. Rev. Lett. **13** (1964) 508. G. S. Guralnik, C. R. Hagen and T. W. B. Kibble, Phys. Rev. Lett. **13**, (1964) 585. F. Englert and R. Brout, Phys. Rev. Lett. **13** (1964) 321.
 - [3] J. Brau *et al.* [ILC Collaboration], arXiv:0712.1950 [physics.acc-ph]. A. Djouadi, J. Lykken, K. Monig, Y. Okada, M. J. Oreglia and S. Yamashita, “International Linear Collider Reference Design Report Volume 2: PHYSICS AT arXiv:0709.1893 [hep-ph]. N. Phinney, N. Toge and N. Walker, arXiv:0712.2361 [physics.acc-ph]. T. Behnke *et al.* [ILC Collaboration], arXiv:0712.2356 [physics.ins-det].
 - [4] V. I. Telnov, Acta Phys. Polon. B **37** (2006) 633 [arXiv:physics/0602172].

- [5] E. Boos *et al.*, Nucl. Instrum. Meth. A **472**, 100 (2001) [arXiv:hep-ph/0103090].
- [6] J. F. Gunion and H. E. Haber, in Research Directions for the Decade, Proceedings of the Summer Study on high energy physics, Snowmass, Colorado, 1990, edited by E. L. Berger (World Scientific, Singapore, 1992), p.469.
- [7] J. F. Gunion and H. E. Haber, Phys. Rev. D **48**, (1993) 5109.
- [8] D. L. Borden, D. A. Bauer and D. O. Caldwell, Phys. Rev. D **48**, 4018 (1993); D. L. Borden, V. A. Khoze, W. J. Stirling and J. Ohnemus, Phys. Rev. D **50**, 4499 (1994).
- [9] M. M. Muhlleitner, M. Kramer, M. Spira and P. M. Zerwas, Phys. Lett. B **508**, (2001) 311. M. M. Muhlleitner, arXiv:hep-ph/0008127.
- [10] D. M. Asner, J. B. Gronberg and J. F. Gunion, Phys. Rev. D **67**, (2003) 035009.
- [11] R. N. Hodgkinson, D. Lopez-Val and J. Sola, arXiv:0901.2257 [hep-ph]; A. Arhrib, R. Benbrik and C. W. Chiang, Phys. Rev. D **77**, 115013 (2008) [arXiv:0802.0319 [hep-ph]]; A. Arhrib, R. Benbrik and C. W. Chiang, AIP Conf. Proc. **1006** (2008) 112; G. Ferrera, J. Guasch, D. Lopez-Val and J. Sola, PoS **RADCOR2007**, 043 (2007) [arXiv:0801.3907 [hep-ph]]; G. Ferrera, J. Guasch, D. Lopez-Val and J. Sola, Phys. Lett. B **659**, 297 (2008) [arXiv:0707.3162 [hep-ph]]. M. N. Dubinin and A. V. Semenov, Eur. Phys. J. C **28**, 223 (2003) [arXiv:hep-ph/0206205].
- [12] G. V. Jikia, Nucl. Phys. B **412**, 57 (1994).
- [13] R. Belusevic and G. Jikia, Phys. Rev. D **70**, 073017 (2004) [arXiv:hep-ph/0403303].
- [14] F. Cornet and W. Hollik, Phys. Lett. B **669**, 58 (2008) [arXiv:0808.0719 [hep-ph]].
- [15] E. Asakawa, D. Harada, S. Kanemura, Y. Okada and K. Tsumura, arXiv:0809.0094 [hep-ph].
- [16] S. H. Zhu, C. S. Li and C. S. Gao, Phys. Rev. D **58**, 015006 (1998) [arXiv:hep-ph/9710424].
- [17] Y. J. Zhou, W. G. Ma, H. S. Hou, R. Y. Zhang, P. J. Zhou and Y. B. Sun, Phys. Rev. D **68**, 093004 (2003) [arXiv:hep-ph/0308226].
- [18] S. H. Zhu, J. Phys. G **24** (1998) 1703.
- [19] G. J. Gounaris and P. I. Porfyriadis, Eur. Phys. J. C **18** (2000) 181 [arXiv:hep-ph/0007110].
- [20] G. Abbiendi *et al.* [OPAL Collaboration], Eur. Phys. J. C **40** (2005) 317 [arXiv:hep-ex/0408097]. J. Abdallah *et al.* [DELPHI Collaboration], Eur. Phys. J. C **38**, 1 (2004) [arXiv:hep-ex/0410017]. S. Schael *et al.* [ALEPH, DELPHI, L3 and OPAL Collaborations], Eur. Phys. J. C **47** (2006) 547.
- [21] J. F. Gunion, H. E. Haber, G. L. Kane and S. Dawson, “THE HIGGS HUNTER’S

- GUIDE,” (Addison–Wesley, Reading, 1990).
- [22] A. Djouadi, Phys.Rept.459:1-241,2008. arXiv:hep-ph/0503173.
 - [23] S. L. Glashow and S. Weinberg, Phys. Rev. D **15** (1977) 1958.
 - [24] V. D. Barger, J. L. Hewett and R. J. N. Phillips, Phys. Rev. D **41** (1990) 3421.
 - [25] T. P. Cheng and M. Sher, Phys. Rev. D **35** (1987) 3484. D. Atwood, L. Reina and A. Soni, Phys. Rev. D **55** (1997) 3156; R. Diaz, R. Martinez and J. A. Rodriguez, Phys. Rev. D **63** (2001) 095007; A. E. Carcamo, R. Martinez and J. A. Rodriguez, Eur. Phys. J. C **50** (2007) 935.
 - [26] H. E. Haber, G. L. Kane and T. Sterling, Nucl. Phys. B **161**, 493 (1979); J. F. Gunion, R. Vega and J. Wudka, Phys. Rev. D **42**, 1673 (1990); J. L. Basdevant, E. L. Berger, D. Dicus, C. Kao and S. Willenbrock, Phys. Lett. B **313**, 402 (1993); V. D. Barger, N. G. Deshpande, J. L. Hewett and T. G. Rizzo, P. Bamert and Z. Kunszt, Phys. Lett. B **306**, 335 (1993); A. G. Akeroyd, Phys. Lett. B **368**, 89 (1996); M. C. Gonzalez-Garcia, S. M. Lietti and S. F. Novaes, Phys. Rev. D **57**, 7045 (1998); A. Barroso, L. Brucher and R. Santos, Phys. Rev. D **60**, 035005 (1999).
 - [27] J. F. Gunion and H. E. Haber, Phys. Rev. D **67**, 075019 (2003) [arXiv:hep-ph/0207010].
 - [28] A. Arhrib and G. Moultaka, Nucl. Phys. B **558**, 3 (1999) [arXiv:hep-ph/9808317].
 - [29] C. Amsler *et al.* [Particle Data Group], Phys. Lett. B **667**, 1 (2008).
 - [30] A. Denner, R. J. Guth, W. Hollik and J. H. Kuhn, Z. Phys. C **51**, 695 (1991).
 - [31] A. W. El Kaffas, O. M. OGREID and P. Osland, arXiv:0709.4203 [hep-ph]. A. Wahab El Kaffas, P. Osland and O. Magne OGREID, Phys. Rev. D **76**, 095001 (2007).
 - [32] M. Misiak and M. Steinhauser, Nucl. Phys. B **764** 62 (2007).
 - [33] A. G. Akeroyd and C. H. Chen, Phys. Rev. D **75**, 075004 (2007) [arXiv:hep-ph/0701078]. C. H. Chen and C. Q. Geng, JHEP **0610**, 053 (2006).
 - [34] K. Ikado *et al.*, Phys. Lett. **97**, 251802 (2006);
 - [35] P. M. Ferreira, R. Santos and A. Barroso, Phys. Lett. B **603** (2004) 219 [Erratum-ibid. B **629** (2005) 114] [arXiv:hep-ph/0406231].
 - [36] S. Kanemura, T. Kubota and E. Takasugi, Phys. Lett. B **313**, 155 (1993); A. G. Akeroyd, A. Arhrib and E. M. Naimi, Phys. Lett. B **490**, 119 (2000); A. Arhrib, arXiv:hep-ph/0012353. J. Horejsi and M. Kladiva, Eur. Phys. J. C **46**, 81 (2006).
 - [37] T. Hahn, Comput. Phys. Commun. **140**, 418 (2001); T. Hahn, C. Schappacher, Comput. Phys.

- Commun. **143**, 54 (2002); J. Küblbeck, M. Böhm, A. Denner, Comput. Phys. Commun. **60**, 165 (1990).
- [38] T. Hahn and J. I. Illana, arXiv:0708.3652 [hep-ph]. T. Hahn and J. I. Illana, Nucl. Phys. Proc. Suppl. **160** (2006) 101; T. Hahn, M. Perez-Victoria, Comput. Phys. Commun. **118**, 153 (1999); T. Hahn and J. I. Illana, arXiv:0708.3652 [hep-ph]. T. Hahn, Nucl. Phys. Proc. Suppl. **89**, 231 (2000).
- [39] G. J. van Oldenborgh, Comput. Phys. Commun. **66**, 1 (1991); T. Hahn, Acta Phys. Polon. B **30**, 3469 (1999).
- [40] T. Hahn, Comput. Phys. Commun. **168** (2005) 78 [arXiv:hep-ph/0404043]. T. Hahn, Nucl. Instrum. Meth. A **559** (2006) 273 [arXiv:hep-ph/0509016].
- [41] A. F. Zarnecki, Acta Phys. Polon. B **34** (2003) 2741; B. Badelek *et al.* [ECFA/DESY Photon Collider Working Group], Int. J. Mod. Phys. A **19** (2004) 5097.
- [42] A. Heister *et al.* [ALEPH Collaboration], Phys. Lett. B **544**, 16 (2002).
- [43] P. Abreu *et al.* [DELPHI Collaboration], Phys. Lett. B **507**, 89 (2001); Eur. Phys. J. C **35**, 313 (2004).
- [44] P. Achard *et al.* [L3 Collaboration], Phys. Lett. B **534**, 28 (2002); Phys. Lett. B **568**, 191 (2003).
- [45] G. Abbiendi *et al.* [OPAL Collaboration], Phys. Lett. B **544**, 44 (2002).
- [46] A. Rosca, arXiv:hep-ph/0212038v1 (2002).
- [47] B. Abbott *et al.* [D0 Collaboration], Phys. Rev. Lett. **82**, 2244 (1999).
- [48] T. Affolder *et al.* [CDF Collaboration], Phys. Rev. D **64**, 092002 (2001).
- [49] http://www-cdf.fnal.gov/physics/exotic/r2a/20081031.diphoton_higgs_fermiophobic/
- [50] V. M. Abazov *et al.* [D0 Collaboration], Phys. Rev. Lett. **101** (2008) 051801 [arXiv:0803.1514 [hep-ex]].
- [51] I. F. Ginzburg, M. Krawczyk, P. Osland, Nucl. Instrum. Meth. A **472**, (2001) 149.
- [52] A. Arhrib, W. Hollik, S. Penaranda and M. Capdequi Peyranere, Phys. Lett. B **579** (2004) 361.
- [53] S. Kanemura, S. Kiyoura, Y. Okada, E. Senaha and C. P. Yuan, Phys. Lett. B **558** (2003) 157; S. Kanemura, Y. Okada, E. Senaha and C. P. Yuan, Phys. Rev. D **70** (2004) 115002.
- [54] L. Brucher and R. Santos, Eur. Phys. J. C **12**, 87 (2000); A. G. Akeroyd, M. A. Diaz and M. A. Rivera, Phys. Rev. D **76**, 115012 (2007).

- [55] S. Kanemura, S. Moretti, Y. Mukai, R. Santos and K. Yagyu, arXiv:0901.0204 [hep-ph].
- [56] A. Arhrib, R. Benbrik, R. B. Guedes and R. Santos, Phys. Rev. D **78** (2008) 075002.